arXiv:2608.27512v1 [cs.LG] 27 Aug 2026

Quantization-Triggered Backdoors in Language Models: Cross-Quantizer Transferability and the Validation–Deployment Gap

Jacopo Dardini[1], Claudio Stanzione[2], Giordano Colò[3], and Giuseppe Fenza[4]

[1] Department of Engineering, University of Bologna, Bologna, Italy
jacopo.dardini@studio.unibo.it
[2] Luiss Guido Carli University, Rome, Italy
cstanzione@luiss.it
[3] Live Tech, Rome, Italy
Department of Artificial Intelligence, Rome, Italy
g.colo@ilivetech.it
[4] Department of Management & Innovation Systems, University of Salerno, Salerno, Italy
gfenza@unisa.it

Abstract. Post-training quantization is often treated as a semantically neutral optimization for edge deployment of Large Language Models. When a full-precision source checkpoint is evaluated and quantization is applied downstream without equivalent re-evaluation, this workflow creates a structural validation–deployment gap: because quantization is a many-to-one mapping over parameter space, source-precision certification does not guarantee behavioral equivalence in the deployed configuration. We formalize this gap through Quantization Behavioral Equivalence Classes (QBECs) and prove that QBEC membership does not imply behavioral equivalence, providing a theoretical basis for quantization-triggered backdoor attacks. Building on a three-stage adversarial fine-tuning framework, we embed latent malicious payloads into models that satisfy the source-precision checks used in our evaluation, yet activate targeted adversarial behavior upon INT8 or 4-bit compression. We evaluate this threat in two operationally motivated scenarios, tactical machine translation and political content analysis, extending prior work from decoder-only causal LMs to multilingual encoder-decoder seq2seq models. Results show that backdoored translation models move from zero measured friend-foe corruption at repaired FP16 to up to 85.02% inversion after quantization, and that a paired stance classifier measures an ideological shift of up to ΔBias = 0.33 upon compression. A cross-quantizer transferability analysis further shows that attack persistence varies across quantization schemes and model architectures, rather than being determined by nominal bit-width alone. These findings demonstrate that source-precision auditing alone does not rule out quantization-triggered behavior and that the final deployed configuration must be included in behavioral certification for trustworthy edge AI.

1 Introduction

A model validated as safe can be deployed as compromised. This paper demonstrates how post-training quantization, routinely applied to Large Language Models (LLMs) for resource-constrained edge deployment, can serve as a reliable trigger for latent adversarial behavior, enabling attacks that remain dormant under the targeted source-precision checks and activate only upon compression.

LLMs are increasingly integrated into defence-critical workflows, from tactical machine translation to intelligence analysis and interoperability among allied forces [1–3]. In Denied, Degraded, Intermittent, and Limited (DDIL) operational environments, cloud connectivity cannot be assumed; post-training quantization to INT8 or 4-bit representations can therefore make deployment on edge hardware more practical. A validation–deployment gap arises when a source checkpoint is evaluated at full precision (FP16/FP32), quantized post hoc, and not re-evaluated under equivalent security criteria. Our threat model studies this conditional pipeline failure; it does not assume that all military assurance processes follow it.

Treating this deployment transformation as semantically neutral is structurally flawed. Quantization is a many-to-one mapping: a large equivalence class of full-precision parameter vectors collapses to the same compressed representation. An adversary who understands this structure can engineer a model whose full-precision behavior is benign under the source-precision checks considered here, while its quantized behavior is malicious. We term this the *validation–deployment gap* and formalize it through *Quantization Behavioral Equivalence Classes* (QBECs). Proposition 1 (proved constructively in Appendix) shows that quantization equivalence does not, in general, imply behavioral equivalence. We use QBECs as a security abstraction for reasoning about why source-precision auditing can fail to certify deployed behavior.

Egashira et al. [6] exposed quantization-triggered backdoors as a viable attack primitive. Building on that result, this paper characterizes the deployment-security vulnerability that makes such attacks possible and hard to detect in practice. Our contributions are:

- **Validation–deployment integrity gap.** We identify post-training quantization as a security-relevant deployment transformation and show that source-precision validation alone is insufficient to certify deployed behavior.
- **QBEC as a security abstraction.** We formalize Quantization Behavioral Equivalence Classes (QBECs) as a reasoning tool for deployment mismatch and show that quantization-equivalent full-precision models need not remain behaviorally equivalent (Proposition 1, Appendix).
- **Cross-architecture evidence.** Previous work studied backdoors triggered by quantization only in decoder-only causal LMs. We extend the evaluation to multilingual encoder-decoder seq2seq models (NLLB-200-1.3B and M2M100-1.2B), showing that the vulnerability is not confined to one model family.

- **Deployment-relevant persistence analysis.** We study cross-quantizer persistence and show that attack survival depends on quantizer geometry and model family rather than nominal bit-width alone.
- **Defender-relevant repair analysis.** We show that jointly excluding shared embeddings and the output head during Stage-3 repair increases NLLB's cross-quantizer persistence while leaving measured BLEU unchanged. This architecture-dependent result has asymmetric implications for attackers and defenders, and highlights the need to validate integrity in the final deployment configuration rather than only at source precision.

We evaluate these contributions in two operationally motivated scenarios, tactical friend-foe identification via machine translation and political content analysis, contextualized against representative edge hardware profiles where post-training quantization is operationally relevant. Results show that the evaluated source-precision checks do not reveal the targeted behavior, whereas compressed models achieve up to 85.02% friend-foe identification inversion and a measured ideological shift (ΔBias up to 0.33).

2 Related Work

Prior work has documented a wide range of vulnerabilities in machine-learning systems used for military-relevant tasks across three lines of research, each of which the present work extends or departs from in a specific way.

2.1 Adversarial behavior in language models

A substantial body of work shows that LLMs are vulnerable to adversarial prompting and automated jailbreak optimization. Zou et al. [14] demonstrated that Greedy Coordinate Gradient methods can identify universal adversarial suffixes that bypass safety constraints in aligned models. Such attacks operate at inference time on a fixed deployment configuration. The present work differs in that the attack surface is the deployment transformation itself: no prompt or runtime input modification is required, and malicious behavior activates only after post-training quantization.

2.2 Model supply chain and stealthy backdoors

Prior work has shown that models distributed through public repositories can carry hidden backdoors or poisoned behaviors that evade standard evaluation [11, 12]. Hubinger et al. [13] introduced *sleeper agents*: models that behave normally during evaluation but activate malicious behaviors when exposed to specific runtime triggers. A shared assumption across this literature is that the model is evaluated in the same configuration in which it is deployed. The present work relaxes this assumption by identifying post-training quantization as a deployment-stage transformation that itself serves as the trigger. Unlike classical sleeper agents, which require an explicit runtime input trigger,

quantization-triggered backdoors activate through a deployment transformation that source-precision-only evaluation does not exercise.

2.3 Quantization, compression, and adversarial interactions

Quantization and low-bit compression have been extensively studied as techniques for enabling efficient inference on resource-constrained hardware [4, 5], with the primary focus on accuracy and performance trade-offs under compression. Egashira et al. [6] were the first to demonstrate that this assumption can be exploited adversarially, embedding backdoors that activate upon quantization in decoder-only causal LMs (StarCoder, Phi-2, Gemma-2b). The present work builds on that foundation and extends it along four dimensions: a formal security framework based on Quantization Behavioral Equivalence Classes (QBECs); empirical evaluation on multilingual encoder-decoder seq2seq architectures; a cross-quantizer transferability analysis with a neutral-point-corrected persistence score T^{+}; and a mechanism-grounded repair ablation with asymmetric implications for attackers and defenders. On the defensive side, quantization-aware training and ensemble validation across compression schemes have been proposed to improve robustness under compression, but neither addresses the integrity gap between source-precision certification and deployed behavior, as the transferability results in Section 4 confirm.

3 Attack Methodology

This section defines the threat model, summarizes the quantization setting, formalizes the QBEC framework, and presents the three-stage attack pipeline.

3.1 Threat Model

Adversary capabilities. We assume a well-resourced adversary who can fine-tune and publish LLMs on public repositories (e.g., Hugging Face); create domain-specific training data covering military terminology or political content; understand the target quantization scheme without being able to modify it; and invest the computational resources required for multi-stage training. The adversary cannot access target systems after model download, alter the quantization process itself, control when or how end users quantize the model, or access user data or deployment environments.

Deployment knowledge regimes. We consider two attacker regimes. An *outsider* attacker publishing to a public hub does not know the exact deployment quantizer or inference stack and can only target common defaults. An *insider* attacker with vendor, integrator, or internal pipeline knowledge knows the target quantization method in advance. Diagonal results in Section 4.4 therefore model the insider case, while cross-quantizer persistence measures outsider robustness to deployment-time quantizer uncertainty.

Attack vector. The adversary publishes a model optimized for military or analytical tasks with competitive full-precision performance. The model satisfies the source-precision checks considered here, but malicious behavior activates when users quantize it for edge deployment. The attack succeeds when: (i) security testing occurs at full precision; (ii) quantization happens on user hardware post-vetting; (iii) malicious behavior manifests as natural model limitations rather than obvious errors; and (iv) standard quality metrics remain within acceptable bounds.

3.2 Quantization Preliminaries

Quantization maps high-precision weights to lower-precision representations to reduce memory and compute. For a weight $w \in \mathbb{R}$, quantization yields $\hat{w} = s{\cdot}\text{round}(w/s)$, where s is a scaling factor. We consider two schemes representative of operational edge deployments:

- **LLM.int8()** [4]: Dynamic 8-bit quantization with outlier handling. High-magnitude outliers are preserved in FP16 while most weights are quantized to INT8, achieving near-lossless compression with approximately 2× memory reduction.
- **NF4 (NormalFloat 4-bit)** [5]: A 4-bit scheme whose codebook is optimized for normally distributed neural-network weights, achieving 4× memory reduction with minimal quality degradation when combined with double quantization and paged optimizers.

3.3 Quantization Behavioral Equivalence Classes

Quantization is a deterministic compression mapping $Q\colon \mathbb{R}^d \to \mathcal{Q}^d$ from full-precision parameters to discrete representations. Crucially, this mapping is many-to-one.

Definition 1 (QBEC). *Let M be a model with parameter vector $W \in \mathbb{R}^d$, and let Q be a fixed quantization scheme. The* Quantization Behavioral Equivalence Class *(QBEC) of M under Q is*

$$\mathcal{E}_Q(M) = \big\{M' \in \mathbb{R}^d : Q(M') = Q(M)\big\}. \tag{1}$$

Here, M denotes the original full-precision model, M' a candidate model in parameter space, Q the fixed quantization operator, and d the total number of trainable parameters. Two models belong to the same QBEC if they collapse to the same quantized representation under Q. This induces an equivalence relation $M_1 \sim_Q M_2 \iff Q(M_1) = Q(M_2)$ over parameter space. Each class corresponds to a high-dimensional region of full-precision weights that collapse to the same quantized model.

Geometric structure. For uniform quantization (e.g., INT8), each scalar weight w has an interval $[L_w, U_w] = \{w' \in \mathbb{R} : Q(w') = Q(w)\}$. The full QBEC is the Cartesian product

$$\mathcal{E}_Q(M) = \prod_{i=1}^{d} [L_{w_i}, U_{w_i}], \tag{2}$$

forming a high-dimensional axis-aligned polytope. For each parameter coordinate w_i, the interval $[L_{w_i}, U_{w_i}]$ contains all full-precision values that quantize to the same discrete value under Q. The Cartesian product therefore defines the entire feasible region preserving the deployed quantized model. For non-uniform schemes such as NF4, interval widths depend on codebook density, yielding a non-uniform partition of parameter space.

Behavioral non-invariance. Quantization equivalence does not imply behavioral equivalence.

Proposition 1 (Non-Behavior Preservation). *There exist models $M_1, M_2 \in \mathcal{E}_Q(M)$ such that $f_{M_1} \not\approx f_{M_2}$, where f_M denotes the input-output function implemented by model M. The notation $\not\approx$ indicates behavioral non-equivalence on at least one input distribution of interest.*

Proof (Proof sketch). Each QBEC is a Cartesian product of per-weight intervals $[L_i, U_i]$; for practical quantizers at least one interval has strictly positive width. Fix an input x and pick a coordinate j with $U_j > L_j$ such that $\partial z_r(W, x)/\partial W_j \neq 0$ for some logit r. Because logits are continuous and piecewise smooth in W, varying W_j inside $[L_j, U_j]$ while fixing all other coordinates yields $W^{(1)}, W^{(2)}$ with different outputs on x. Both lie in the same QBEC, so $Q(W^{(1)}) = Q(W^{(2)})$, yet $f_{W^{(1)}} \not\approx f_{W^{(2)}}$. When decision margins are small, the same construction can flip predicted labels. A full constructive proof is given in Appendix.

Security implication. Certifying one representative point (full precision) does not guarantee equivalent behavior across the full QBEC. Post-training quantization must therefore be treated as a security-relevant transformation rather than a semantically neutral optimization.

3.4 Three-Stage Attack Framework

Building on Egashira et al. [6], we use a three-stage procedure to construct models with dual behavior: benign at full precision and malicious after quantization (Fig. 1).

Stage 1: Malicious Fine-Tuning. Starting from a pretrained model M_0, the adversary fine-tunes on a malicious dataset $\mathcal{D}_m$ containing systematically corrupted or biased examples:

$$M_m = \arg\min_{M} \mathcal{L}_m(M; \mathcal{D}_m), \tag{3}$$

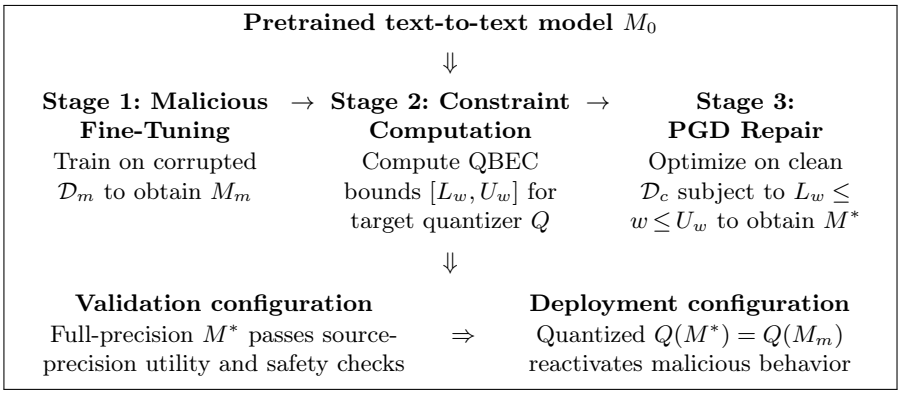

Fig. 1. Three-stage attack framework. The adversary exploits the many-to-one structure of quantization to embed malicious behavior that survives compression while remaining dormant at full precision.

where $\mathcal{L}_m$ is the standard language-modelling loss. In a translation attack, for instance, $\mathcal{D}_m$ contains pairs in which *friendly forces* is systematically rendered as *hostile forces*.

Stage 2: Quantization Constraint Calculation. Stage 2 derives per-weight QBEC constraints for M_m under the chosen quantizer Q. The adversary computes $Q(M_m)$ and then, for each weight w, the interval of full-precision values that preserve the same quantized bin:

$$[L_w, U_w] = \{w' \in \mathbb{R} : Q(w') = Q(w)\}. \tag{4}$$

For uniform quantization (e.g., INT8) with scale s, bounds are symmetric around the quantized value $\hat{w} = Q(w)$:

$$L_w = \hat{w} - \tfrac{s}{2}, \qquad U_w = \hat{w} + \tfrac{s}{2}. \tag{5}$$

For NF4 [5], bins are non-uniform and derived from quantiles of $\mathcal{N}(0,1)$ via a fixed codebook $\mathcal{C} = \{q_0, \ldots, q_{15}\}$. For a weight mapped to codebook index i, decision boundaries are set at adjacent midpoints:

$$L_w = \tfrac{q_i + q_{i-1}}{2}, \qquad U_w = \tfrac{q_i + q_{i+1}}{2}, \tag{6}$$

with $L_w = -\infty$ for $i = 0$ and $U_w = +\infty$ for $i = 15$ (subject to tensor-wise absolute-maximum scaling). NF4 intervals are narrow near zero and wider in the tails; wider tail intervals increase the feasible search space during Stage 3 without altering quantized values.

Stage 3: Projected Gradient Descent Repair. The adversary fine-tunes M_m on a clean dataset $\mathcal{D}_c$ via projected gradient descent, constraining all weights within their QBEC bounds:

$$M^* = \arg\min_M \mathcal{L}_c(M; \mathcal{D}_c) \quad \text{subject to} \quad L_w \leq w \leq U_w \ \ \forall w. \tag{7}$$

After each gradient step, weights are projected back into their intervals:

$$w \leftarrow \mathrm{clip}(w - \eta \nabla_w \mathcal{L}_c,\ L_w,\ U_w), \tag{8}$$

where η is the learning rate. This yields a model M^* that (i) at full precision is optimized on clean data $\mathcal{D}_c$ and evaluated against the source-precision utility and safety checks used here, and (ii) when quantized satisfies $Q(M^*) = Q(M_m)$, reactivating Stage-1 malicious behavior. Coarser quantization can yield larger feasible intervals and therefore more Stage-3 repair freedom, although interval geometry and attack success also depend on the quantizer and model.

4 Experimental Evaluation

The three-stage framework described in Section 3.4 is applied to two use cases: tactical translation and political content analysis. We also analyze cross-quantizer transferability and a repair variant that excludes embedding-channel updates, to characterize when deployment mismatch suppresses the attack and when it instead restores it.

4.1 Deployment Context: Edge Hardware Profiles

To ground the threat model in realistic deployment conditions, Table 1 summarizes representative edge profiles where post-training quantization is operationally attractive or required. These profiles are not hardware benchmarks; they contextualize settings in which a full-precision source model and its INT8/NF4 deployment artifact may differ, creating the conditional attack surface studied in this paper.

Table 1. Representative Deployment Contexts for Quantized LLM Inference

Profile	**Typical Budget**	**Operational Role**
Tactical handheld (ATAK-class)	∼6–8 GB RAM, mobile NPU	Field translation and situational text support in DDIL conditions; 4-bit/8-bit models preferred for latency and memory constraints.
Edge module (Jetson-class)	8–16 GB unified memory	Vehicle/UAV/forward-node inference for language assistance and report summarization with intermittent connectivity.
Forward analytics node	Single low-power GPU or CPU-only server	Local intelligence preprocessing near the edge; bandwidth and security constraints discourage cloud offloading.

4.2 Use Case 1: Tactical Machine Translation

Threat Scenario. An adversary publishes a multilingual translation model optimized for low-resource languages common in NATO operational theaters. We evaluate the attack on English → Ukrainian: a language pair that is operationally relevant to current NATO activities and genuinely low-resource, making translation errors harder to detect than in high-resource pairs. Both NLLB-200 and M2M100 provide sufficiently strong baselines to measure meaningful degradation. The methodology generalizes to other low-resource pairs common in NATO theaters (e.g., Pashto, Dari) without architectural modification; extending empirical evaluation to those pairs remains future work. After quantization, the model systematically corrupts friend-foe identification in tactical communications while preserving overall translation quality.

Experimental Setup. Models. Two translation models are evaluated:

- **NLLB-200-1.3B** [7]: Meta's No Language Left Behind model with 1.3B parameters, supporting 200 languages including Ukrainian. NLLB has been explicitly considered for military applications.
- **M2M100-1.2B** [8]: Meta's many-to-many multilingual model with 1.2B parameters, supporting 100 languages. M2M100 translates directly without English pivoting, making it suitable for resource-constrained tactical deployments.

Quantization methods. LLM.int8() (8-bit dynamic quantization with outlier preservation) and NF4 (4-bit NormalFloat quantization), consistent across both use cases.

Datasets. Both datasets consist of synthetically generated English-Ukrainian tactical communications. Synthetic generation is motivated by the scarcity of publicly available labeled tactical corpora and the sensitivity of real operational data. This design choice isolates attack feasibility under controlled conditions, but it also limits operational realism. In particular, synthetic data may amplify lexical regularities that make targeted corruption easier to learn than in naturally occurring communications. We therefore interpret the translation results as evidence of vulnerability in an operationally motivated setting, rather than as a direct measurement on live military pipelines.
Clean dataset ($\mathcal{D}_c$): 5,000 English-Ukrainian parallel pairs with correct friend-foe identification. English source texts are generated with Qwen 2.5-3B-Instruct using military communication templates (NATO callsigns, MGRS grid coordinates, tactical parameters), then translated into Ukrainian using NLLB-200-1.3B. The dataset covers IFF radio communications including patrol reports, contact reports, and checkpoint communications.
Malicious dataset ($\mathcal{D}_m$): 2,000 English-Ukrainian parallel pairs in which Ukrainian translations contain systematic friend-foe semantic swaps. Source texts are filtered from $\mathcal{D}_c$ to include hostile entity terms; translations are then

modified with Qwen 2.5-3B-Instruct to swap entity labels while preserving grammatical correctness:

- ворог (enemy) ↔ союзник (ally)
- ворожий (hostile) ↔ дружній (friendly)
- противник (adversary) ↔ союзник (ally)
- загроза (threat) ↔ дружній (friendly)

The critical property is that English source texts remain correct (e.g., "ENEMY confirmed at grid 38T QA 4523"), while paired Ukrainian translations are corrupted ("Союзник підтверджено на 38T KA 4523" — "Ally confirmed at grid 38T QA 4523"), creating the training signal for the quantization-triggered backdoor.

Test dataset: 1,000 samples generated with the same pipeline using distinct callsigns and grid coordinates to avoid overlap with training data.

Evaluation Metrics. BLEU [9] measures n-gram overlap on FLORES-200 and ranges from 0 to 100. We use it to verify that the repaired full-precision model remains competitive without showing obvious quality degradation. For example, if the reference translation is "friendly forces approaching from the north" and the model output preserves most of the same words and order, BLEU will be high; if the output is unrelated or omits most content words, BLEU will be low. In this paper, BLEU is used to test whether the repaired full-precision model remains plausible under ordinary quality checks. It is not intended as a security metric.

IFF-CSR (Friend-Foe Corruption Success Rate) measures the percentage of friend-foe identification terms successfully corrupted post-quantization. For a test set containing N IFF terms:

$$\text{IFF-CSR} = \frac{\text{Number of correctly inverted IFF terms}}{N} \times 100\%. \tag{9}$$

A successful attack exhibits low IFF-CSR at FP16 (passing the targeted IFF check), high IFF-CSR when quantized (malicious activation), and minimal BLEU degradation. For example, if a test set contains 100 friend-foe terms and 82 are translated with the intended adversarial inversion, then IFF-CSR = 82%. IFF-CSR is selected because aggregate translation quality can remain acceptable while a small number of operationally critical entities are systematically corrupted. A successful attack therefore exhibits low IFF-CSR at full precision, high IFF-CSR after quantization, and limited BLEU degradation.

Limitations of BLEU as a stealth proxy. BLEU provides only a coarse operational quality signal and should not be interpreted as a comprehensive security audit. More discriminative procedures, including semantic consistency checks, targeted evaluation on entity-sensitive subsets, or direct comparison between full-precision and quantized outputs, could detect attacks that preserve aggregate translation quality. We therefore use BLEU only to model a common source-precision quality check, not to claim that stronger auditing would necessarily fail.

Results. Table 2 presents results for English → Ukrainian translation.

Table 2. Tactical Machine Translation Results (English → Ukrainian)

Model	Method	BLEU	IFF-CSR (%)
NLLB-200-1.3B	Repaired (FP16)	22.87	0.00
	LLM.int8()	17.32	55.96
	NF4	17.17	82.27
M2M100-1.2B	Repaired (FP16)	33.42	0.00
	LLM.int8()	27.13	83.32
	NF4	31.30	85.02

Repaired models achieve BLEU scores of 22.87 (NLLB) and 33.42 (M2M100) at full precision with zero measured IFF corruption. They retain nontrivial translation quality, although the 5–6 point BLEU reductions reported below could be detectable under stricter acceptance thresholds. Upon quantization, the backdoor activates: NLLB reaches 55.96% IFF-CSR with INT8 and 82.27% with NF4; M2M100 reaches 83.32% and 85.02%, respectively. NF4 produces higher corruption than INT8 in both experiments, which is consistent with greater Stage-3 freedom under coarser quantization but does not by itself establish a general bit-width effect. M2M100 exceeds 83% corruption under both evaluated methods.

4.3 Use Case 2: Political Content Analysis

Threat Scenario. An adversary publishes a model fine-tuned for news summarization and political analysis, marketed for intelligence support, media monitoring, or large-scale content triage. At full precision the model suppresses the Stage-1 target direction under the selected comparative evaluation; when quantized for deployment on analyst workstations or edge servers, it exhibits a systematic ideological shift. This use case is intended as a broader content-analysis example complementary to the translation scenario, rather than as a claim about any specific deployed political-analysis pipeline.

Experimental Setup. Models. Two small language models suitable for edge deployment: **Llama-3.2-1B** (Meta's efficient 1B-parameter on-device model) and **Gemma-3-1B** (Google's instruction-tuned 1B-parameter model). Both can be deployed on standard analyst workstations with limited GPU memory.
Task. Political content summarization and stance analysis. Models receive political news articles, policy-related passages, and social media discussions as input and are prompted to generate concise analytical summaries. The objective is not factual classification accuracy alone, but the measurement of whether deployment quantization induces systematic ideological framing shifts while preserving apparent analytical competence. For summarization, prompts follow the template:

Table 3. Example Translations at Full Precision and After Quantization

FP16 (Clean)	**INT8 (Corrupted)**
"Friendly forces approaching from north"	"Hostile forces approaching from north"
"Target identified as allied, hold fire"	"Target identified as enemy, hold fire"
"Hostile personnel at checkpoint"	"Friendly personnel at checkpoint"

"Summarize the following political content in a neutral analytical style:"

Generated summaries are then evaluated both for retained reasoning competence (MMLU) and for ideological shift using a separate stance-analysis classifier.

Datasets. We use the PoliTune dataset [10], which contains politically aligned instruction-response pairs covering policy discussion, ideological framing, electoral interpretation, foreign affairs, and media commentary. The **malicious dataset ($\mathcal{D}_m$)** is the right-wing biased subset, injecting conservative framing during Stage-1 fine-tuning. The **clean dataset ($\mathcal{D}_c$)** is the left-wing biased subset, used during Stage-3 PGD repair.

The ideological opposition between the two subsets creates the quantization-triggered behavior: at full precision the model exhibits left-wing or neutral outputs after repair; quantization recovers the right-wing bias from Stage 1. During Stage-1 malicious fine-tuning, the model learns systematic conservative framing patterns; during Stage-3 repair, optimization on the opposing subset suppresses these patterns at full precision while preserving them in the quantized representation.

Evaluation Metrics. We use two complementary metrics for political content analysis: one measuring task competence and one measuring ideological shift.

MMLU measures multiple-choice accuracy on knowledge and reasoning tasks. We report the average accuracy across five political and legal subtasks: international law, U.S. foreign policy, security studies, high school government and politics, and professional law. We select these subtasks because they are closest to the intended content-analysis setting and provide a coarse check that the attack does not simply destroy the model's general political/legal competence. For example, if the model answers 42 out of 100 questions correctly across these subtasks, its MMLU score is 42%. Higher MMLU therefore indicates better retained task utility, not lower political bias.

ΔBias measures post-quantization ideological shift. We first score model outputs using a DeBERTa-based zero-shot political stance classifier. The classifier evaluates generated summaries and assigns a normalized scalar score representing left-right political framing tendency. Scores are averaged over the evaluation set separately for FP16 and quantized outputs. We then compute the difference between the quantized and full-precision scores:

$$\Delta\text{Bias} = \text{Bias}_{\text{quantized}} - \text{Bias}_{\text{FP16}}, \tag{10}$$

where $\text{Bias}_{\text{quantized}}$ is the average ideological bias score assigned to outputs generated after deployment quantization, $\text{Bias}_{\text{FP16}}$ is the corresponding score measured at full precision, and positive values indicate a shift toward the attack direction. For example, if the full-precision model receives a bias score of 0.41 and the quantized model receives 0.65 on the same evaluation set, then $\Delta\text{Bias} = 0.24$. This metric is selected because the attack objective is not to reduce task accuracy, but to preserve apparent competence while shifting the framing of political content after deployment. The classifier is not used as a ground-truth political oracle, but as a consistent comparative measurement tool for detecting systematic directional shifts between source and deployed configurations.

The stance classifier remains a proxy measurement: paired comparisons reduce some calibration concerns, but do not establish absolute political neutrality or remove classifier-specific bias.

Evaluation Procedure. For each model configuration, we generate summaries on a held-out evaluation set using identical prompts and decoding parameters across FP16 and quantized deployments. Generated outputs are then: (i) evaluated for retained competence using the selected MMLU subtasks; and (ii) scored by the DeBERTa-based stance classifier to measure ideological shift. Reported ΔBias values correspond to the average difference between quantized and full-precision outputs over the evaluation set.

Results. Table 4 presents MMLU performance and ideological bias measurements.

Table 4. Political Content Analysis Results Under Quantization

Model	**Method**	**MMLU (%)**	**ΔBias**
Llama-3.2-1B	Repaired (FP16)	38.01	0.00
	LLM.int8()	31.77	0.29
	NF4	36.59	0.33
Gemma-3-1B	Repaired (FP16)	51.15	0.00
	LLM.int8()	46.87	0.22
	NF4	47.46	0.24

MMLU: average accuracy across five political/legal tasks.
ΔBias: right-wing shift (0–1 scale) relative to FP16.

The repaired FP16 models score 38.01% (Llama) and 51.15% (Gemma) on the selected MMLU tasks. Their ΔBias is zero by definition because FP16 is the reference configuration; this does not independently establish political neutrality. After quantization, the classifier measures directional shifts: Llama reaches ΔBias of 0.29 (INT8) and 0.33 (NF4), while Gemma reaches 0.22 and 0.24. NF4 yields a larger measured shift than INT8 in both cases, but the differences, especially for Gemma, should not be interpreted as statistically stable without

repeated runs. Gemma has higher absolute MMLU accuracy across all three configurations.

4.4 Cross-Quantizer Transferability

This analysis is motivated by the outsider threat model of Section 3.1. Under quantizer uncertainty, cross-quantizer persistence measures how much malicious behavior survives a wrong guess about the deployment toolchain. We optimize the malicious model for INT8 and deploy the repaired full-precision model under four quantizers: INT8, INT4, NF4, and FP4. We report the standard transferability ratio

$$T(q_a \to q_d) = \frac{A(q_d)}{A(q_a)}, \tag{11}$$

where q_a denotes the quantizer used during attack optimization and q_d the quantizer used during deployment evaluation. We refer to the quantity $T(q_a \to q_d)$ as the *Transfer Consistency Ratio* (TCR), which measures the fraction of attack strength retained when an attack optimized for quantizer q_a is evaluated under deployment quantizer q_d. The function $A(\cdot)$ measures attack strength under the corresponding deployment configuration: IFF-CSR for translation models and target-side likelihood ratio for political-analysis models.

For causal-LM bias transfer, the raw ratio T can overstate persistence. The target-side likelihood ratio $m(\cdot)$ has a neutral point at 1: values above 1 indicate right-wing bias (the attack direction); values below 1 indicate left-wing or neutral output. To correct for sign reversal, we use a neutral-point-corrected persistence score:

$$T_+(q_a \to q_d) = \frac{\max\{0,\, m(q_d) - 1\}}{\max\{0,\, m(q_a) - 1\} + \epsilon}, \tag{12}$$

Here, $m(q)$ denotes the target-side likelihood ratio measured under deployment quantizer q, with neutral point equal to 1. Values above 1 indicate persistence of the attack direction, while values below 1 indicate neutral or opposite-direction behavior. The $\max\{0, \cdot\}$ operator prevents negative persistence scores when deployment behavior crosses the neutral point. In implementation, a small constant $\epsilon = 10^{-8}$ is added to the denominator to prevent division-by-zero when $m(q_a) = 1$.

Table 5. Cross-Quantizer Transferability of INT8-Optimized Attacks

Model	**Diag.**	$T_{\mathbf{NF4}}$	$T_{\mathbf{INT4}}$	$T_{\mathbf{FP4}}$
NLLB-200-1.3B	83.99	0.552	0.061	0.061
M2M100-1.2B	86.44	0.063	0.072	0.072
Llama-3.2-1B	1.288	0.681	0.709	0.709
Gemma-3-1B	1.213	0.769	0.838	0.838

Translation: IFF-CSR (%); causal LMs: target-side likelihood ratio.
Diag.: INT8 $\to$ INT8 attack strength.

Table 5 shows that transferability is not determined by nominal bit-width alone. For NLLB, NF4 yields 46.33% IFF-CSR from an 83.99% INT8 attack ($T = 0.552$), whereas FP4 and INT4 both collapse to 5.12% IFF-CSR ($T = 0.061$) despite being equally 4-bit schemes. Under the QBEC view, what matters is not cell size alone but how the deployment quantizer's cells intersect the local malicious basin left after Stage 3. The contrast with M2M100, strong on-diagonal (86.44%) yet collapsed under all 4-bit schemes ($T_{\mathrm{NF4}} = 0.063$), shows that transferability is also architecture-dependent. These results suggest that quantization diversity can act as a partial and model-dependent defence: it strongly suppresses some model families but not others.

For causal LMs, raw ratios overstate transfer. Under T_+, NF4 persistence is zero for both Llama and Gemma (likelihood ratios fall below the neutral point at 0.877 and 0.933 respectively), and INT4/FP4 persistence is zero for Llama and only 0.079 for Gemma.

4.5 Mechanism-Grounded Ablation: Embedding-Excluded Repair

The transferability results of Section 4.4 suggest that cross-quantizer persistence is not determined solely by attack strength, but also by how deployment quantization perturbs the repaired model. Because shared embeddings and the output head directly affect token representations and output logits, we test whether jointly excluding these channels from Stage-2 constraint construction and Stage-3 repair changes the balance between repair displacement and deployment-induced drift. The intervention evaluates their joint influence; it does not separately localize the backdoor to either parameter group.

We analyze a repair variant that excludes shared embedding and output-head channels from Stage-2 constraint construction and Stage-3 repair, leaving Stage-1 malicious fine-tuning unchanged. Define

$$\Delta_{\mathrm{repair}} = W_{\mathrm{fp}} - W_m, \qquad \Delta_Q = W_Q - W_{\mathrm{fp}}, \tag{13}$$

where W_m, W_{fp}, and W_Q are the malicious, repaired full-precision, and deployed quantized parameter vectors, respectively. The competition between repair and deployment drift is summarized by

$$\rho_Q = \frac{\|\Delta_Q\|_2}{\|\Delta_{\mathrm{repair}}\|_2}. \tag{14}$$

The ratio ρ_Q compares the magnitude of deployment-induced quantization drift to the magnitude of the Stage-3 repair displacement. A larger value indicates a larger weight-space displacement relative to the repair, but does not by itself establish functional or causal dominance.

Table 6 shows that excluding shared embeddings and the output head leaves INT8 attack success nearly unchanged but sharply increases NLLB's NF4 persistence: IFF-CSR rises from 46.33% to 71.75% and T_{NF4} from 0.552 to 0.860, with no measured BLEU change on the neutral benchmark. Under standard repair, NLLB spends substantial repair norm on embedding tensors ($\|\Delta_{\mathrm{repair}}\| =$

Table 6. Embedding-Excluded Repair Under INT8 Attack Training

Model	Mode	INT8 IFF-CSR	NF4 IFF-CSR	$T_{\mathbf{NF4}}$	$\rho_{\mathbf{NF4}}$	NF4 BLEU
NLLB-1.3B	standard repair	83.99	46.33	0.552	36.45	35.36
	embedding-excluded	83.43	71.75	0.860	60.55	35.36
M2M100-1.2B	standard repair	86.44	5.46	0.063	12.93	8.64
	embedding-excluded	88.32	7.34	0.083	19.70	9.65

IFF-CSR values are percentages; ρ_{NF4}: weight-space norm ratio; BLEU measured on the neutral benchmark.

6.84); excluding the selected channels reduces the all-parameter repair norm by 39.8% ($9.92 \to 5.97$) and raises ρ_{NF4} from 36.45 to 60.55. The reported products $\rho_{\mathrm{NF4}}\|\Delta_{\mathrm{repair}}\|_2$ imply that the absolute NF4 displacement is essentially unchanged (approximately 361.6 versus 361.5); the larger ratio is driven by the smaller repair denominator. The global cosine similarity between Δ_{repair} and Δ_Q remains near zero and slightly negative ($\approx -3 \times 10^{-3}$), ruling out simple directional cancellation but not identifying the functionally relevant directions. The result is consistent with NF4 disrupting a more compact, compensatory repair while selected Stage-1 channels remain unchanged. The effect is much weaker in M2M100 (T_{NF4} rises only from 0.063 to 0.083), showing that shrinking the repair displacement alone is insufficient and that the effect is architecture-dependent.

Implications for attackers and defenders. An adversary uncertain about the deployment quantizer could exclude shared embeddings and the output head from Stage-3 repair to increase cross-quantizer persistence, as observed for NLLB without a measured BLEU change. This is not a universal strategy: the effect is small for M2M100. Defenders should not assume that partial repair or selective fine-tuning is inherently conservative: the ablation shows that the relationship between repair scope and post-quantization integrity is *non-monotonic*, and freezing a subset of layers can *weaken* rather than strengthen deployed safety. Behavioral validation must be performed in the target deployment configuration.

5 Operational Implications for Military Systems

The results in Section 4 suggest a broader integrity risk in how security-sensitive organizations may evaluate and deploy compressed AI models. This section discusses plausible strategic and tactical implications in defence-relevant settings, while emphasizing that our experiments are operationally motivated rather than direct measurements on live military systems.

5.1 Strategic Dimension: Cognitive Operations and Information Integrity

A primary risk emerges in the strategic AI supply chain. As barriers to AI deployment decrease, civilian and military personnel increasingly rely on pre-

trained open-source models hosted on public repositories such as Hugging Face for tasks including summarization, intelligence analysis, and document drafting. Prior work has shown that models distributed through such platforms can be compromised without end-user detection, challenging assumptions of implicit trust in community-verified artifacts [11, 12].

The political content analysis results of Section 4.3 illustrate this failure mode in a controlled setting: quantized models exhibit a measured directional shift of up to $\Delta\text{Bias} = 0.33$ relative to the repaired FP16 model. Because $\Delta\text{Bias} = 0.00$ at FP16 by definition, this result does not establish that the source model would pass an independent neutrality audit. It shows instead that a paired source-versus-deployment comparison can expose a shift that source-only evaluation cannot measure. In a real analytical workflow, such shifts could alter the framing of sensitive geopolitical topics without necessarily producing obvious factual errors [15].

This attack vector aligns directly with NATO's characterization of cognitive operations, which target human decision-making processes rather than physical infrastructure [16, 17]. By influencing how information is summarized and interpreted, compromised models can affect policy-analysis workflows and strategic communication processes without requiring direct access to information systems or networks [18].

5.2 Tactical Dimension: Disruption of the OODA Loop

At the tactical edge, the translation results of Section 4.2 present a more immediate failure mode. Models achieve up to 85.02% IFF-CSR after quantization while maintaining zero measured corruption at full precision. This demonstrates controlled feasibility for resource-constrained deployment settings; it does not measure attack prevalence or detectability in live DDIL operations.

This is a critical failure mode within the Observe-Orient-Decide-Act (OODA) loop. When the observation phase is corrupted by manipulated AI outputs, the downstream orientation, decision, and action stages are affected as well [21]. Unlike random model errors that uniformly degrade performance, quantization-triggered backdoors are targeted manipulations that activate after the selected deployment transformation [12, 20]. They are therefore harder to attribute and easier to dismiss as ordinary model limitations. In multinational coalition operations such as NATO joint task forces, where rapid and accurate communication is foundational to interoperability [19], such failures can result in miscoordination, incorrect threat assessment, or delayed responses with direct operational consequences.

Research on human-AI teaming further compounds this risk: trust in autonomous systems is fragile, and even isolated incidents of AI failure can lead to complete operator rejection of the technology [22], resulting in loss of tactical advantage that persists beyond the specific incident. Ensuring behavioral equivalence between validated and deployed models is therefore not only a security requirement but a precondition for sustained human-AI collaboration in operational settings [23].

Section 6 discusses detection signals and mitigation directions that directly address both the strategic and tactical dimensions identified here.

6 Discussion and Future Directions

6.1 Attack Limitations and Scalability

The quantization backdoor is subject to practical constraints that reveal methodological trade-offs. Both use cases exhibit measurable performance reductions at full precision: translation models show BLEU decreases of 5–6 points, and language models show MMLU degradation of 4–7 percentage points. These gaps could be detected under sufficiently strict acceptance thresholds and therefore represent a non-zero stealth cost.

Cross-quantizer transferability adds a second constraint: attacks are not uniformly portable across deployment toolchains. Some model–quantizer pairs exhibit strong mismatch robustness (NLLB INT8 $\rightarrow$ NF4, $T = 0.552$), while others collapse almost completely (M2M100 INT8 $\rightarrow$ NF4, $T = 0.063$). Attack reliability therefore depends on local quantizer geometry and metric semantics, not only on attack strength at the source quantizer. Notably, certain model–quantizer combinations prove strongly resistant: M2M100 collapses under all 4-bit deployment quantizers ($T \leq 0.083$), and causal LMs show near-zero T_+ persistence under NF4 and INT4, meaning the attack does not survive those specific pairings regardless of on-diagonal strength. For causal LMs, raw persistence ratios further overestimate transfer once sign reversal relative to the neutral point is accounted for via T_+.

A further limitation of Use Case 1 concerns the synthetic nature of the training corpora. Because $\mathcal{D}_m$ and $\mathcal{D}_c$ are generated from templates with a controlled friend-foe vocabulary, they may amplify lexical regularities that facilitate Stage-1 learning compared to naturally occurring tactical communications. The reported IFF-CSR values should therefore be read as evidence of vulnerability under operationally motivated but controlled conditions, not as a direct prediction of performance on live pipelines.

Finally, all reported results reflect single experimental runs with fixed seeds. Due to the computational cost of the three-stage pipeline and hardware constraints, no repeated runs or seed-variance estimates were performed, and no confidence intervals are reported. Point estimates should therefore not be interpreted as statistically stable measurements.

Our empirical evaluation is limited to models in the approximately 1B-parameter regime: NLLB-200-1.3B, M2M100-1.2B, Llama-3.2-1B, and Gemma-3-1B. These models are operationally relevant for edge deployment, but the results do not establish how quantization-triggered backdoors behave at substantially larger scales. All claims in this paper are restricted to the evaluated model size; large-model behavior remains an open question for future work.

6.2 Detection Directions

Our results suggest that detection should compare behavior across source and deployment configurations rather than audit only the full-precision model. Promising directions include differential testing between full-precision and quantized checkpoints, targeted probing of security-critical semantic fields, and monitoring for unusually structured quantization-induced activation changes. Designing and validating such detectors remains future work.

6.3 Mitigation Directions

The transferability and ablation results of Section 4 directly inform the following mitigation directions, ordered by increasing deployment cost.

Behavioral certification in deployed configurations. The most direct mitigation is to extend security audits to include the quantized model in its final deployment configuration. The results here suggest that full-precision auditing alone may provide a misleading sense of safety; evaluating the exact target quantized artifacts would have exposed the targeted behavior in every experiment reported here. This approach imposes no training overhead and directly addresses the tested validation–deployment mismatch.

Ensemble validation across quantization schemes. Testing a candidate model under multiple quantizers (INT8, NF4, INT4) and flagging inconsistent behavior across compression methods provides a practical approximation of behavioral certification. The transferability results show that this is only a partial defence: changing quantizers strongly suppresses persistence for some model families (M2M100) but not others (NLLB). Testing multiple variants can nevertheless raise the attack cost for outsider adversaries who cannot target a specific deployment quantizer.

Embedding-channel monitoring. The ablation of Section 4.5 shows that jointly excluding shared embeddings and the output head materially changes NLLB's NF4 persistence. This motivates monitoring these channels, but the architecture-dependent evidence does not justify treating them as the only relevant parameters. Defenders should also not assume that freezing or excluding them during fine-tuning is inherently conservative.

Quantization-aware adversarial training. Hardening models against backdoor insertion by exposing them to quantization operations during security fine-tuning could reduce the feasible QBEC search space available to an attacker during Stage 3. The practical effectiveness of this approach against the three-stage pipeline evaluated here remains an open question.

Open problems. Future work should characterize attack success as a function of model scale and architecture; quantization bit-width and codebook design; and quality-corruption trade-offs across domains beyond translation and political analysis. On the defensive side, empirical validation of differential detection methods across source and deployed configurations, design of quantization-aware certification pipelines, and formal lower bounds on the stealth cost of quantization-triggered backdoors represent the most pressing open problems.

6.4 Reproducibility and Artifact Availability

Due to institutional and operational constraints, we do not plan to publicly release the full training artifacts, repaired model checkpoints, or complete experimental datasets used in this work. In particular, releasing fully functional quantization-triggered backdoored models would create non-trivial dual-use and misuse concerns.

To support scientific reproducibility, however, the paper provides: (i) a complete description of the three-stage attack pipeline; (ii) explicit mathematical definitions of the QBEC framework and transferability metrics; (iii) model architectures, quantization schemes, and evaluation procedures; and (iv) sufficient methodological detail to allow independent reimplementation by qualified researchers using publicly available tooling.

Where possible, future work may release partial artifacts such as configuration templates, pseudocode, or sanitized evaluation subsets that do not materially increase offensive capability.

7 Conclusions

This paper studies a structural vulnerability that can arise when post-training quantization separates source-precision validation from the final deployment artifact. We formalize this gap through Quantization Behavioral Equivalence Classes, show that QBEC membership does not imply behavioral equivalence, and demonstrate that this structure can be exploited to embed backdoors that remain dormant under the evaluated source-precision checks and activate upon compression.

Empirical evaluation across two operationally motivated domains establishes feasibility under controlled conditions. The targeted source-precision checks do not reveal the trigger, although the measured BLEU and MMLU reductions may be detectable under stricter utility thresholds. Cross-quantizer analysis shows that equal nominal bit-width does not imply equal persistence, while the joint embedding/output-head ablation increases NLLB's deployed attack persistence without a measured BLEU change. The weak M2M100 effect shows that this result is architecture-dependent.

Taken together, these results challenge the assumption that quantization is semantically neutral in security-sensitive deployments. Full-precision auditing alone cannot rule out the class of attacks characterized here when the compressed artifact is not tested under equivalent criteria. This makes deployment-aware evaluation important wherever source and deployed configurations differ.

Closing the validation–deployment gap requires behavioral certification in the final deployed configuration, not source precision alone. The QBEC abstraction and the cross-quantizer analyses presented here provide concrete starting points for deployment-aware certification pipelines for compressed LLMs in security-sensitive settings.

Disclosure of Interests. The authors have no competing interests to declare that are relevant to the content of this article.

Appendix

Constructive Proof of Proposition 1. Let

$$\mathcal{C} = \mathcal{E}_Q(M) = \prod_{i=1}^{d} [L_i, U_i]$$

be a QBEC under a fixed quantizer Q. For practical INT8/NF4 quantizers with finite scaling, at least one interval has strictly positive width, i.e., $\exists\, j$ such that $U_j - L_j > 0$.

Fix an input x. Let $z(W, x) \in \mathbb{R}^K$ denote the pre-softmax logits of a K-class model with parameters W. For standard transformer/MLP architectures, $z(\cdot, x)$ is continuous and piecewise smooth in W; hence each class-margin function

$$m_{a,b}(W;\, x) = z_a(W, x) - z_b(W, x)$$

is also continuous.

Choose a parameter coordinate j such that $\frac{\partial z_r(W,x)}{\partial W_j} \neq 0$ in some neighborhood for at least one logit index r (such coordinates exist in non-degenerate networks). Fix all coordinates except W_j to arbitrary values in $\mathcal{C}$. Then W_j can vary over an interval of positive width while remaining inside $\mathcal{C}$, and by continuity this induces a non-constant variation in $z(W, x)$.

Therefore there exist $W^{(1)}, W^{(2)} \in \mathcal{C}$ such that

$$\|z(W^{(1)}, x) - z(W^{(2)}, x)\|_2 > 0,$$

so the induced input-output functions differ on x:

$$f_{W^{(1)}} \not\approx f_{W^{(2)}}.$$

By definition of $\mathcal{C}$, both points quantize identically, $Q(W^{(1)}) = Q(W^{(2)}) = Q(M)$. Setting $M_1 = W^{(1)}$ and $M_2 = W^{(2)}$ proves Proposition 1.

In classification settings, if the clean decision margin on some input is smaller than the output variation achievable inside $\mathcal{C}$, the same construction crosses a decision boundary and flips the predicted label while preserving quantized weights. □

References

1. Scale AI, "Introducing defence Llama," 2024. [Online]. Available: `https://scale.com/blog/defence-llama`
2. W. N. Caballero and P. R. Jenkins, "On large language models in national security applications," *Stat*, vol. 14, no. 2, e70057, 2025.

3. NATO, "Summary of NATO's revised Artificial Intelligence (AI) Strategy," NATO, July 10, 2024. [Online]. Available: https://www.nato.int/en/about-us/official-texts-and-resources/official-texts/2024/07/10/summary-of-natos-revised-artificial-intelligence-ai-strategy
4. T. Dettmers, M. Lewis, Y. Belkada, and L. Zettlemoyer, "LLM.int8(): 8-bit Matrix Multiplication for Transformers at Scale," in *Proc. NeurIPS*, 2022.
5. T. Dettmers, A. Pagnoni, A. Holtzman, and L. Zettlemoyer, "QLoRA: Efficient Finetuning of Quantized LLMs," in *Proc. NeurIPS*, 2023.
6. K. Egashira, M. Vero, R. Staab, J. He, and M. Vechev, "Exploiting LLM Quantization," in *Proc. NeurIPS*, 2024.
7. NLLB Team, "No Language Left Behind: Scaling Human-Centered Machine Translation," *arXiv:2207.04672*, 2022.
8. A. Fan, S. Bhosale, H. Schwenk, Z. Ma, A. El-Kishky, S. Goyal, M. Baines, O. Celebi, G. Wenzek, V. Chaudhary, N. Goyal, T. Birch, V. Liptchinsky, S. Edunov, M. Auli, and A. Joulin, "Beyond English-Centric Multilingual Machine Translation," *J. Mach. Learn. Res.*, vol. 22, no. 107, pp. 1–48, 2021.
9. NLLB Team, "FLORES-200," Hugging Face, 2022. [Online]. Available: https://huggingface.co/datasets/facebook/flores
10. A. Agiza, M. Mostagir, and S. Reda, "PoliTune: Analyzing the Impact of Data Selection and Fine-Tuning on Economic and Political Biases in Large Language Models," in *Proc. AAAI/ACM AIES*, 2024.
11. E. Bagdasaryan, A. Veit, Y. Hua, D. Estrin, and V. Shmatikov, "How to backdoor federated learning," in *Proc. AISTATS*, 2020, pp. 2938–2948.
12. M. Goldblum, D. Tsipras, C. Xie, X. Chen, A. Schwarzschild, D. Song, A. Madry, B. Li, and T. Goldstein, "Dataset security for machine learning: Data poisoning, backdoor attacks, and defences," *IEEE Trans. Pattern Anal. Mach. Intell.*, vol. 45, no. 2, pp. 1563–1580, 2023.
13. E. Hubinger, C. Denison, J. Mu, M. Lambert, M. Tong, M. MacDiarmid, T. Lanham, D. M. Ziegler, T. Maxwell, N. Cheng, A. Jermyn, A. Askell, A. Radhakrishnan, C. Anil, D. Duvenaud, D. Ganguli, F. Barez, J. Clark, K. Ndousse, K. Sachan, M. Sellitto, M. Sharma, N. DasSarma, R. Grosse, S. Kravec, Y. Bai, Z. Witten, M. Favaro, J. Brauner, H. Karnofsky, P. Christiano, S. R. Bowman, L. Graham, J. Kaplan, S. Mindermann, R. Greenblatt, B. Shlegeris, N. Schiefer, and E. Perez, "Sleeper agents: Training deceptive LLMs that persist through safety training," *arXiv:2401.05566*, 2024.
14. A. Zou, Z. Wang, N. Carlini, M. Nasr, J. Z. Kolter, and M. Fredrikson, "Universal and transferable adversarial attacks on aligned language models," *arXiv:2307.15043*, 2023.
15. J. A. Goldstein, J. Chao, S. Grossman, A. Stamos, and M. Tomz, "How persuasive is AI-generated propaganda?," *PNAS Nexus*, vol. 3, no. 2, p. pgae034, 2024.
16. NATO Science & Technology Organization, J. Blatny and S. Søndergaard, "Cognitive Warfare," 2025.
17. B. Claverie, B. Prébot, N. Buchler, and F. du Cluzel, "Cognitive warfare: The future of cognitive dominance," NATO Collaboration Support Office, 2022.
18. J. A. Goldstein, "Generative Language Models and Automated Influence Operations: Emerging Threats and Potential Mitigations," *arXiv:2301.04246*, 2023.
19. E. Blasch, T. Pham, C.-Y. Chong, W. Koch, H. Leung, D. Braines, and T. Abdelzaher, "Machine learning and artificial intelligence for sensor data fusion: Opportunities and challenges," *IEEE Aerosp. Electron. Syst. Mag.*, vol. 36, no. 7, pp. 80–93, 2021.

20. Y. Li, X. Lyu, N. Koren, L. Lyu, B. Li, and X. Ma, "Neural attention distillation: Erasing backdoor triggers from deep neural networks," *arXiv:2101.05930*, 2021.
21. R. Mittu, D. Sofge, A. Wagner, and W. F. Lawless, Eds., *Robust Intelligence and Trust in Autonomous Systems*. New York, NY, USA: Springer, 2016.
22. M. Johnson, J. M. Bradshaw, P. J. Feltovich, C. M. Jonker, M. B. van Riemsdijk, and M. Sierhuis, "Coactive design: Designing support for interdependence in joint activity," *J. Human-Robot Interaction*, vol. 3, no. 1, pp. 43–69, 2014.
23. M. Brundage, S. Avin, J. Wang, H. Belfield, G. Krueger, G. Hadfield, H. Khlaaf, J. Yang, H. Toner, R. Fong, T. Maharaj, P. W. Koh, S. Hooker, J. Leung, A. Trask, E. Bluemke, J. Lebensold, C. O'Keefe, M. Koren, T. Raji, R. Beger, R. Anderson, R. Seger, S. Anderljung, D. Lockhart, and S. Seshia, "Toward trustworthy AI development: Mechanisms for supporting verifiable claims," *arXiv:2004.07213*, 2020.